

Article

Comparison of MOCVD and MBE Regrowth for CAVET Fabrication

Simon Kotzea ^{1,*}, Wiebke Witte ¹, Birte-Julia Godejohann ², Mathias Marx ^{1,3},
Michael Heuken ^{1,3}, Holger Kalisch ¹ and Rolf Aidam ² and Andrei Vescan ¹

¹ Compound Semiconductor Technology (CST), RWTH Aachen University, Sommerfeldstr. 18, 52074 Aachen, Germany; wiebke-witte@posteo.de (W.W.); M.Marx@aixtron.com (M.M.); M.Heuken@aixtron.com (M.H.); kalisch@cst.rwth-aachen.de (H.K.); vescan@cst.rwth-aachen.de (A.V.)

² Fraunhofer-Institut für Angewandte Festkörperphysik (IAF), Tullastr. 72, 79108 Freiburg, Germany; birte-julia.godejohann@ise.fraunhofer.de (B.-J.G.); Rolf.Aidam@iaf.fraunhofer.de (R.A.)

³ AIXTRON SE, Dornkaulstr. 2, 52134 Herzogenrath, Germany

* Correspondence: simon.kotzea@cst.rwth-aachen.de

Received: 6 March 2019; Accepted: 23 March 2019; Published: 28 March 2019



Abstract: In this paper, we demonstrate the fabrication of current aperture vertical electron transistors (CAVET) realized with two different epitaxial growth methods. Templates with a p-GaN current blocking layer (CBL) were deposited by metal organic chemical vapor deposition (MOCVD). Channel and barrier layers were then regrown by either molecular beam epitaxy (MBE) or MOCVD. Scanning electron microscope (SEM) images and atomic force microscope (AFM) height profiles are used to identify the different regrowth mechanisms. We show that an AlN interlayer below the channel layer was able to reduce Mg diffusion during the high temperature MOCVD regrowth process. For the low-temperature MBE regrowth, Mg diffusion was successfully suppressed. CAVET were realized on the various samples. The devices suffer from high leakage currents, thus further regrowth optimization is needed.

Keywords: CAVET; current aperture vertical electron transistor; gallium nitride; vertical power devices

1. Introduction

The research on wide-bandgap semiconductor power devices is driven by the need for efficient transistors. The superior material properties of e.g., GaN or SiC allow for higher reverse bias and elevated operating temperature limits, compared to lower-bandgap Si-based devices. Lateral high electron mobility transistors (HEMT) have already entered the market in the medium power conversion range, achieving blocking voltages of 600 V [1]. For high-power applications, a vertical geometry is preferred over a lateral one, particularly due to better scaling possibilities and an improved breakdown voltage. The peak electric field is located in the bulk of the semiconductor for most vertical designs and a more uniform electric field distribution is achieved [2], reducing the need for complex field-plate structures [3]. Several device concepts are currently investigated, such as vertical trench metal oxide semiconductor field effect transistor (FET) [4,5], finFET [6,7] or vertical junction FET [8–10]. Another promising design is the CAVET [11–17]. Here, a two-dimensional electron gas (2DEG) with high carrier mobility is formed above a CBL with an aperture. It combines the mobility advantage of the HEMT with a vertical device design to increase the blocking voltage without enlarging chip size. However, selective doping or etching [18] is necessary in order to fabricate the aperture. While selective air-gap etching moves the peak electric field back to the semiconductor surface, selective doping can be realized by either implantation or regrowth [19]. In this study, we investigate both MOCVD and MBE

regrowth to fabricate CAVET. The growth mechanisms of the two techniques on the patterned aperture region will be compared and evaluated regarding CAVET fabrication and properties.

2. Experiment

Templates for both regrowth techniques were grown on sapphire in an AIXTRON Planetary MOCVD tool. Due to the insulating substrates, a quasi-vertical design has to be employed. Trimethylgallium (TMGa) and ammonia were used as precursors, silane and magnesocene for n- and p-type doping, respectively. The carrier gas was hydrogen. The complete template stack is depicted in Figure 1a. No additional preparation of the sapphire wafers was carried out before growth. After AlN nucleation on sapphire, 2 μm n⁺-GaN were deposited, forming the backside contact layer. Above, a 700-nm-thick drift layer with a doping concentration of $N_D = 5 \times 10^{16} \text{ cm}^{-3}$ was grown. Thickness and N_D were chosen for low R_{ON} with respect to the V_{BR} trade-off [20]. The epitaxial stack was completed with a 250-nm-thick p⁺-GaN layer, possessing a high acceptor concentration of $N_A = 1.3 \times 10^{19} \text{ cm}^{-3}$. This layer serves as CBL.

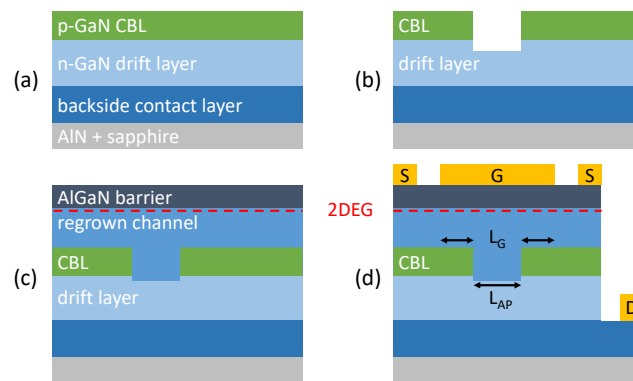


Figure 1. Basic process flow for the fabrication of a CAVET and important parameters for the device geometry. (a) Epitaxial stack of template; (b) Dry etching of aperture; (c) Idealized schematic after MOCVD/MBE regrowth of channel and barrier layer; (d) Backside contact layer exposure and contact deposition.

After template growth, patterned samples were fabricated by etching the aperture into the p-GaN, utilizing a two-step Cl-based etch process (Figure 1b). At first, a high-power inductively coupled plasma reactive-ion etching (ICP-RIE) is employed to expose the drift layer. It was optimized for steep sidewalls [21]. Subsequently, a low-damage cyclic ICP etch process is used to carefully remove etch-damaged material [22]. This second process leads to a smooth surface with low rms roughness of 1.2 nm. Both processes combined yield an etch depth of 300 nm. The templates were dipped in HCl and BOE consecutively for one minute each in order to remove surface contamination and for regrowth preparation [23].

Then, a GaN HEMT structure consisting of a GaN channel layer and an AlGaIn barrier was regrown with MOCVD and MBE, respectively (Figure 1c). The regrowth process fills the previously etched aperture with GaN.

MOCVD regrowth was performed at $T_{\text{growth}} = 1050 \text{ }^\circ\text{C}$ and two samples were prepared (CVD-A and CVD-B). The regrowth of sample CVD-A consists of a 300-nm-thick GaN channel with $N_D = 2 \times 10^{16} \text{ cm}^{-3}$, which was capped by a 25-nm-thick $\text{Al}_{0.25}\text{Ga}_{0.75}\text{N}$ barrier layer. For sample CVD-B, a 5 nm AlN interlayer was regrown below the GaN channel to block Mg-diffusion from the p-GaN CBL [24].

MBE regrowth was carried out at $T_{\text{growth}} = 750 \text{ }^\circ\text{C}$. The lower growth temperature suppresses Mg diffusion [25,26]. Two samples (MBE-C and MBE-D) with different GaN channel thicknesses, but without AlN interlayer, were regrown. Sample MBE-C had a 300-nm-thick channel layer, whereas

sample MBE-D was fabricated with a 450-nm-thick channel. Both were doped with $N_D = 2 \times 10^{16} \text{ cm}^{-3}$ and capped by the same 25-nm-thick $\text{Al}_{0.25}\text{Ga}_{0.75}\text{N}$ barrier. For sample MBE-D, a more conductive 2DEG is expected, due to the increased distance between 2DEG and regrowth interface.

Following the regrowth, CAVET were fabricated (Figure 1d). The backside contact layer was exposed by ICP dry-etching utilizing a 450-nm-thick Cr hard mask. Subsequently, the sample was dipped in diluted HCl before e-beam evaporation of the ohmic contact metals. The drain and source contact stacks, consisting of Ti/Al/Ni/Au (15 nm/100 nm/40 nm/50 nm), were deposited and annealed at 825 °C to ensure an ohmic characteristic. Finally, the Ni/Au (50 nm/200 nm) gate contact was formed on top of the aperture region.

Additionally, three lateral HEMT reference samples without p-GaN CBL were grown. All samples consist of a 300-nm-thick GaN channel layer and a 25 nm $\text{Al}_{0.25}\text{Ga}_{0.75}\text{N}$ barrier layer, analog to the one mentioned above, to serve as reference for a Mg-free (re)growth. The epitaxial layer stack for reference sample 1 was continuously grown with MOCVD. The HEMT structure for reference 2 and 3 was regrown on lowly n-doped GaN templates with MOCVD and MBE, respectively. A brief summary of all fabricated templates is given in Table 1.

Table 1. Samples overview.

Sample	Technique	T_{growth}	Remark
CVD-A	MOCVD	1050 °C	-
CVD-B	MOCVD	1050 °C	5 nm AlN interlayer
MBE-C	MBE	750 °C	300 nm channel
MBE-D	MBE	750 °C	450 nm channel
Ref. 1	MOCVD	1050 °C	continuously grown
Ref. 2	MOCVD	1050 °C	regrown on n-GaN
Ref. 3	MBE	750 °C	regrown on n-GaN

SEM images and AFM surface profiles of the aperture region after regrowth were used to identify the growth mechanisms of the different regrowth techniques on patterned samples. Eddy-current and, after ohmic contact deposition, Hall measurements were conducted to characterize the 2DEG properties. I-V measurements were carried out to investigate the CAVET performance. The contact resistances were determined with transfer length method (TLM) measurements.

3. Results and Discussion

3.1. Structural Characterization

3.1.1. MOCVD Regrowth

Figure 2a shows the MOCVD-regrown region of an 8- μm -wide aperture on sample CVD-A. The previously 300-nm-deep etched aperture, indicated by the dotted line, is completely filled. A narrower imprint of the opening is still visible. AFM depth profiles of the MOCVD-regrown aperture with various widths (L_{AP}) are plotted in Figure 2b, confirming residual trenches after regrowth. The remaining trench depth increases from 40 nm for $L_{\text{AP}} = 2 \mu\text{m}$ to 120 nm for $L_{\text{AP}} = 8 \mu\text{m}$. Also, the sidewall angle θ is increased from 3° to 7° for larger L_{AP} . The growth morphology is different on the sidewalls compared to a planar regrown surface in the vicinity of a trench, as shown in Figure 2d, but rms roughness is similar.

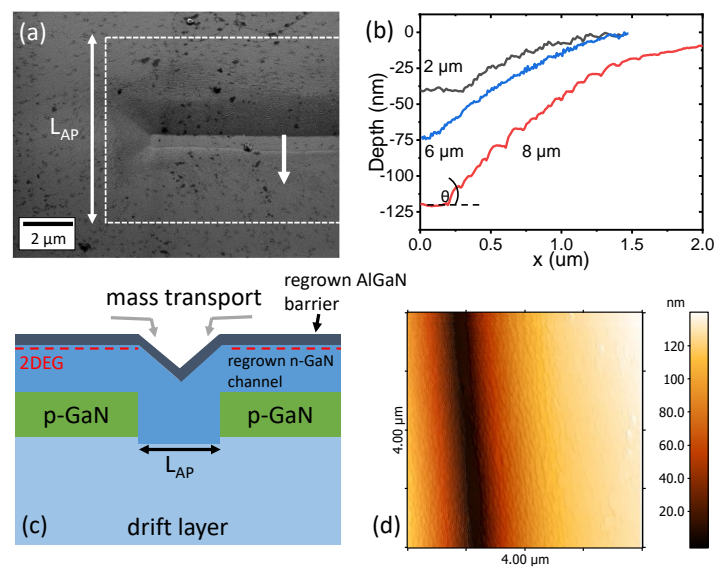


Figure 2. (a) SEM image of an 8- μm -wide aperture region on sample CVD-A after MOCVD regrowth. The aperture opening before regrowth is indicated by the dotted line. The white arrow indicates the direction of the depth profile scan line. (b) Depth profiles of MOCVD-regrown trenches with different L_{AP} and sidewall angle θ . (c) Schematic cross section of the trench after regrowth. (d) AFM scan of aperture region on sample CVD-A.

2D layer growth at the p-GaN surface and the trench bottom dominates for large L_{AP} , forming an imprint of the original trench. But also, mass transport from the p-GaN surface to the trench sidewall is occurring, as indicated in gray in Figure 2c [27]. This leads to small sidewall angles, a different surface morphology and a planarization of the trench. For smaller L_{AP} , this effect increases due to more overlapping growth from each sidewall and results in a smaller imprint with shallower sidewalls, as observed in the AFM profiles in Figure 2b.

To prevent field crowding and leakage currents after the gate contact deposition on top of the aperture region, a planar surface and therefore a small remaining trench with a small sidewall angle is desired. However, by decreasing L_{AP} , the aperture resistance will be increased and a high R_{ON} is to be expected.

3.1.2. MBE Regrowth

For the low-temperature MBE regrowth process, less mass transport from the p-GaN surface into the trenches should occur. SEM images of MBE-regrown apertures in Figure 3a–c confirm this expectation. The schematic cross section in Figure 3d illustrates the growth mechanism. In addition to 2D growth (white arrows), lateral overgrowth can be observed (black arrow). Due to the low temperatures during MBE growth, the diffusion length of the atoms is limited. Thus, lateral growth at the edge is enhanced compared to growth at the bottom of the trench and leads to the formation of a protrusion. For small L_{AP} , this inhibits growth inside of the trench and the formation of the channel layer in the aperture is hindered.

Therefore, a large L_{AP} is necessary, as this will lead to a smaller protrusion and a larger overlap of the material regrown at the aperture edge. Still, the gate contact has to be formed with care to prevent a rupture of the metal layer at the protrusions.

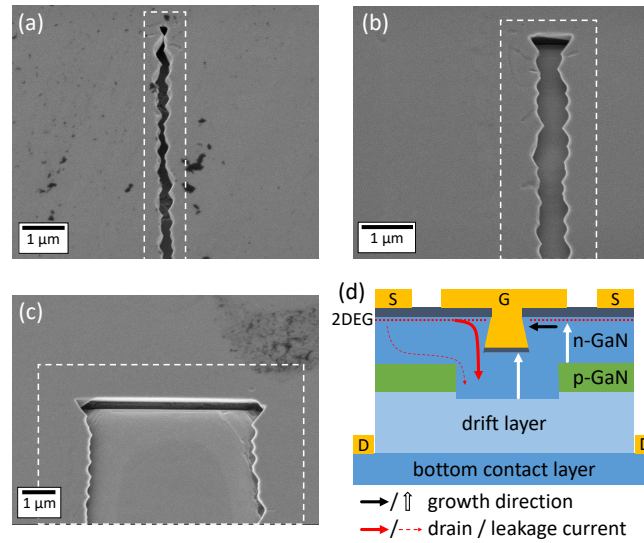


Figure 3. (a–c) SEM images of 1 μm, 2 μm and 8 μm wide aperture regions (L_{AP}) after the regrowth of sample MBE-C. The trench opening before regrowth is indicated by the dotted line. (d) Schematic cross section of MBE regrowth on a patterned sample. The drain current (solid) and source-drain leakage current (dashed) paths are indicated by the red arrows (cf. Section 3.2.3).

3.2. Electrical Characterization

3.2.1. Planar 2DEG Properties

Eddy-current and Hall measurements were carried out to investigate the 2DEG formation in the layers on top of the CBL. Statistics of these measurements of several positions on each sample are presented in Figure 4. All p-GaN samples showed a sheet resistance R_{sheet} in the order of $50,000 \Omega/sq$ before regrowth. The strong decrease of R_{sheet} for all samples cannot solely be explained by regrowing the lowly doped n-GaN channel layer and thus the formation of a 2DEG at the AlGaIn/GaN interface appears plausible. For the continuously MOCVD-grown reference sample 1, the lowest $R_{sheet} = 340 \Omega/sq$ and highest mobility $\mu = 2000 \text{ cm}^2/Vs$ can be extracted. Also, the sheet carrier concentration is $n_s = 10 \times 10^{12} \text{ cm}^{-2}$, which is expected for the given AlGaIn thickness and Al content.

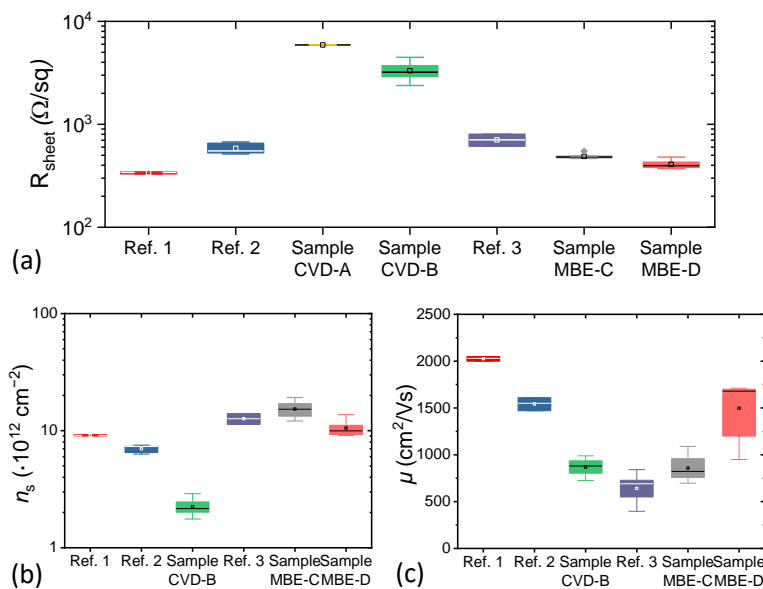


Figure 4. (a) Eddy-current measurement results after regrowth. (b) Sheet carrier concentration n_s and (c) mobility μ extracted from Hall measurements.

A slightly increased R_{sheet} is obtained for the regrown reference sample 2, probably due to increased interface roughness or defect scattering, introduced by the regrowth. Low-temperature Hall measurements at 77 K (not shown here) still reveal a reduced mobility compared to reference sample 1 and confirm the proposed scattering mechanisms, as all other are frozen out at 77 K [28,29].

For the MOCVD-regrown samples on p-GaN, a dramatic increase in R_{sheet} is observed. The highest $R_{\text{sheet}} = 5900 \Omega/\text{sq}$ is obtained for sample CVD-A, as no measures were taken to inhibit Mg diffusion. The AlN interlayer introduced in sample CVD-B is also not able to suppress the Mg diffusion completely, resulting in an increased sheet resistance of $3200 \Omega/\text{sq}$ and reduced $n_{\text{S}} = 2.2 \times 10^{12} \text{ cm}^{-2}$. For sample CVD-A, no Hall data is available.

All MBE-regrown samples (reference 3, MBE-C and MBE-D) achieve the expected $n_{\text{S}} = 10 \times 10^{12} \text{ cm}^{-2}$ and are comparable to reference sample 2 in terms of R_{sheet} . This indicates a successful suppression of Mg diffusion for the low temperature MBE regrowth. The increased mobility for sample MBE-D could be attributed to an improved AlGaIn/GaN interface quality due to a larger distance to the regrowth interface. However, both samples show the same rms surface roughness of 1 nm.

Overall, improved 2DEG properties are achieved with the MBE regrowth, compared to the high-temperature MOCVD regrowth process. The lower T_{growth} suppresses Mg diffusion effectively. Hence, the acceptor concentration near the 2DEG is supposed to be low. The AlN interlayer in CVD-B did improve R_{sheet} and may be a viable option to enable an MOCVD regrowth for CAVET after further optimization. However, the AlN interlayer will introduce an additional energy barrier for the drain current through the aperture when regrown below the channel layer. Therefore, sample CVD-A and MBE-D were chosen to compare the properties of CAVET fabricated with each regrowth technique and are analyzed in the following.

3.2.2. MOCVD-Regrown CAVET (CVD-A)

Deduced from the Hall measurements, a low maximum available drain current is to be expected for the MOCVD-regrown CAVET. Source contacts on top of the AlGaIn barrier show a contact resistance of $R_{\text{C,S}} = 7 \Omega\text{mm}$, the drain contact resistance $R_{\text{C,D}}$ is $1.7 \Omega\text{mm}$. The high $R_{\text{C,S}}$ may be caused by Mg diffusion into the regrown n-GaN.

A CAVET with a gate length of $L_{\text{G}} = 2 \mu\text{m}$ and a $L_{\text{AP}} = 1 \mu\text{m}$ is discussed here (cf. Figure 1 for geometry). All currents are normalized to the active area, which is the distance between the source contacts multiplied by the gate width of $54 \mu\text{m}$.

The output characteristic of the transistor is presented in Figure 5a. V_{GS} was varied from +2 V to -8 V in 1 V steps. No drain current saturation and a delayed turn-ON of the transistor can be observed. Both effects are most likely caused by parasitic series resistances of the 2DEG, aperture and source contacts. A simple DC equivalent circuit model of a CAVET is depicted in Figure 5b and comprises the following resistances: the contact resistances ($R_{\text{C,S}}$, $R_{\text{C,D}}$), the lateral 2DEG resistance R_{2DEG} , the aperture resistance R_{ap} , the drift layer resistance R_{drift} and the backside contact layer resistance R_{bcl} . Our calculations, based on measurements of lumped-element model test structures (e.g., TLM structures and lateral HFETs regrown on CBL with and without aperture), led to an aperture resistance R_{ap} of approx. $10 \text{ M}\Omega$. The reason for this high R_{ap} may be, that the aperture is partially depleted from the lateral p-n junction, formed by the p-GaN CBL and the n-GaN aperture, or Mg has diffused into the regrown aperture during the high temperature MOCVD regrowth, compensating the n-doping. However, the large R_{ap} and low 2DEG conductivity limit the maximum available drain current to $I_{\text{D,max}} = 1.3 \text{ A/cm}^2$ and cause a high turn-ON voltage. The weak pinch-off can be improved by increasing L_{G} , as shown in the inset of Figure 5a. L_{AP} is $6 \mu\text{m}$ for these devices. With a larger L_{G} , the gate control of the regrown GaN is enhanced and the source-drain leakage current is effectively suppressed.

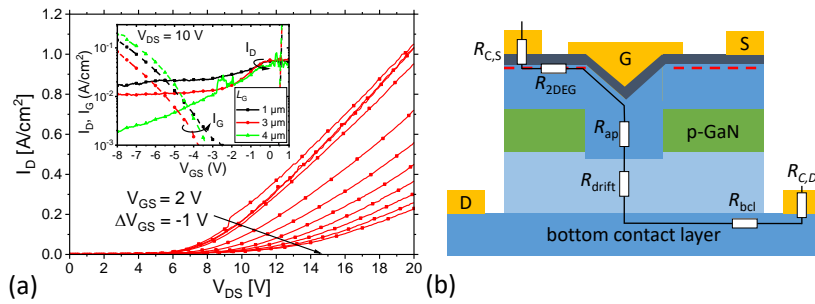


Figure 5. (a) Output characteristic of an MOCVD-regrown CAVET with $L_G = 2 \mu\text{m}$ and $L_{AP} = 1 \mu\text{m}$. Inset: transfer characteristics of transistors with various L_G and $L_{AP} = 6 \mu\text{m}$. (b) DC equivalent circuit model comprising all series resistances.

Destructive breakdown occurs below the gate at $V_{DS} = -140 \text{ V}$. This results in a critical electrical field of $E_{\text{crit}} = 2.8 \text{ MV/cm}$, by assuming a complete depletion of the $1\text{-}\mu\text{m}$ -long gate-drain distance.

3.2.3. MBE-Regrown CAVET (MBE-D)

An improved regrowth quality and lower Mg diffusion are expected for the MBE-regrown CAVET, compared to the CAVET with MOCVD regrowth. The source contact resistance of the MBE-regrown device is $R_{C,S} = 0.4 \Omega\text{mm}$, already indicating a lower Mg concentration at the surface. The drain contact resistance is $R_{C,D} = 2 \Omega\text{mm}$.

The output characteristic of devices with $L_G = 2 \mu\text{m}$ and $L_{AP} = 8 \mu\text{m}$, $6 \mu\text{m}$ and $2 \mu\text{m}$ are depicted in Figure 6a. In contrast to the MOCVD-regrown CAVET, current saturation, a larger maximum drain current density of $I_{D,\text{max}} = 4 \text{ kA/cm}^2$ for $V_{GS} = 2 \text{ V}$ and low $R_{\text{ON}} = 2 \text{ m}\Omega \text{ cm}^2$ are achieved.

Figure 6b shows the transfer characteristics of the same devices. The transistors suffer from high OFF-state and gate leakage currents. Possible OFF-state drain leakage current paths, i.e., along the etched sidewall to the quasi-backside contact and through the CBL, can be excluded, as previous experiments on these building blocks show the suppression of leakage currents [21]. The most probable drain leakage current path for the transistor with $L_{AP} = 8 \mu\text{m}$ is through the lowly doped GaN channel and aperture as indicated in Figure 3d by the dashed arrow. As observed in the previous Section 3.1.2, the overlap between the regrown GaN channel in- and alongside the aperture is reduced for smaller apertures. This cuts off this drain leakage current path at the cost of a smaller $I_{D,\text{max}}$, as can be seen in Figure 6b and increases the ON/OFF ratio to $2.3 \times 10^3 [I_D(V_{GS} = 0 \text{ V})/I_D(V_{GS} = -8 \text{ V})]$ for the device with $L_{AP} = 2 \mu\text{m}$. However, the transistors are still limited by gate leakage currents, probably due to the gate deposition on the non-planarized regrown-aperture region.

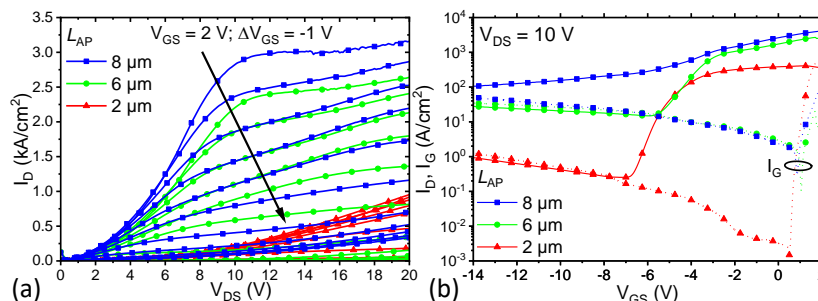


Figure 6. (a) Output characteristics of MBE-regrown CAVET with $L_G = 2 \mu\text{m}$ and $L_{AP} = 8 \mu\text{m}$, $6 \mu\text{m}$ and $2 \mu\text{m}$. (b) Transfer characteristics of the same devices for $V_{DS} = 10 \text{ V}$.

4. Summary and Conclusions

Two different regrowth techniques were used to fabricate CAVET. The regrowth was conducted after aperture patterning on MOCVD-grown CBL with MBE and MOCVD, respectively. MOCVD-regrown aperture regions showed small imprints of the etched aperture opening with small sidewall angles. This was correlated with mass transport into the trench during regrowth. On the other hand, protrusions were formed at apertures after the low-temperature MBE regrowth.

For the high-temperature MOCVD-regrown transistors, no current saturation and low $I_{D,max}$ were measured, which is probably due to Mg diffusion into the regrown aperture.

The MBE-regrown CAVET showed improved ON characteristics but suffered from high gate and OFF-state leakage currents. Regrowth thickness and channel layer doping concentration should be decreased to allow for low drain leakage currents. A planarization of the aperture region or an optimized aperture width to height ratio may also help to suppress leakage currents.

Author Contributions: Conceptualization, W.W., M.M., S.K., H.K. and A.V.; formal analysis, W.W.; investigation, W.W., B.-J.G. and M.M.; supervision, M.H., H.K., R.A. and A.V.; visualization, S.K. and W.W.; writing—original draft, S.K.; writing—review & editing, S.K.

Funding: Funding of BMBF under grant nr. 16ES0147 is acknowledged.

Conflicts of Interest: The authors declare no conflict of interest. The funders had no role in the design of the study; in the collection, analyses, or interpretation of data; in the writing of the manuscript, or in the decision to publish the results.

References

1. Jones, E.A.; Wang, F.F.; Costinett, D. Review of Commercial GaN Power Devices and GaN-Based Converter Design Challenges. *IEEE J. Emerg. Sel. Top. Power Electron.* **2016**, *4*, 707–719. [[CrossRef](#)]
2. Chowdhury, S. GaN-on-GaN power device design and fabrication. In *Wide Bandgap Semiconductor Power Devices*; Elsevier: Amsterdam, The Netherlands, 2019; pp. 209–248.
3. Chowdhury, S.; Mishra, U.K. Lateral and Vertical Transistors Using the AlGaIn/GaN Heterostructure. *IEEE Trans. Electron Devices* **2013**, *60*, 3060–3066. [[CrossRef](#)]
4. Li, W.; Chowdhury, S. Design and fabrication of a 1.2 kV GaN-based MOS vertical transistor for single chip normally off operation. *Phys. Status Solidi* **2016**, *213*, 2714–2720. [[CrossRef](#)]
5. Gupta, C.; Lund, C.; Chan, S.H.; Agarwal, A.; Liu, J.; Enatsu, Y.; Keller, S.; Mishra, U.K. In Situ Oxide, GaN Interlayer-Based Vertical Trench MOSFET (OG-FET) on Bulk GaN substrates. *IEEE Electron Device Lett.* **2017**, *38*, 353–355. [[CrossRef](#)]
6. Sun, M.; Zhang, Y.; Gao, X.; Palacios, T. High-Performance GaN Vertical Fin Power Transistors on Bulk GaN Substrates. *IEEE Electron Device Lett.* **2017**, *38*, 509–512. [[CrossRef](#)]
7. Zhang, Y.; Sun, M.; Piedra, D.; Hu, J.; Liu, Z.; Lin, Y.; Gao, X.; Shepard, K.; Palacios, T. 1200 V GaN vertical fin power field-effect transistors. In Proceedings of the 2017 IEEE International Electron Devices Meeting (IEDM), San Francisco, CA, USA, 2–6 December 2017.
8. Kizilyalli, I.; Aktas, O. Characterization of vertical GaN p-n diodes and junction field-effect transistors on bulk GaN down to cryogenic temperatures. *Semicond. Sci. Technol.* **2015**, *30*, 124001. [[CrossRef](#)]
9. Ji, D.; Chowdhury, S. Design of 1.2 kV Power Switches With Low R_{ON} Using GaN-Based Vertical JFET. *IEEE Trans. Electron Devices* **2015**, *62*, 2571–2578.
10. Kotzea, S.; Debal, A.; Heuken, M.; Kalisch, H.; Vescan, A. Demonstration of a GaN-Based Vertical-Channel JFET Fabricated by Selective-Area Regrowth. *IEEE Trans. Electron Devices* **2018**, *65*, 5329–5336. [[CrossRef](#)]
11. Ben-Yaacov, I. AlGaIn/GaN Current Aperture Vertical Electron Transistors. Ph.D. Thesis, University of California, Santa Barbara, CA, USA, 2004.
12. Ben-Yaacov, I.; Seck, Y.K.; Mishra, U.K.; DenBaars, S.P. AlGaIn/GaN current aperture vertical electron transistors with regrown channels. *J. Appl. Phys.* **2004**, *95*, 2073–2078. [[CrossRef](#)]
13. Chowdhury, S. Aluminum Gallium Nitride/Gallium Nitride CAVETs for High Power Switching Application. Ph.D. Thesis, University of California, Santa Barbara, CA, USA, 2010.

14. Chowdhury, S.; Wong, M.H.; Swenson, B.L.; Mishra, U.K. CAVET on Bulk GaN Substrates Achieved With MBE-Regrown AlGa_N/GaN Layers to Suppress Dispersion. *IEEE Electron. Device Lett.* **2012**, *33*, 41–43. [[CrossRef](#)]
15. Mandal, S.; Agarwal, A.; Ahmadi, E.; Bhat, K.M.; Ji, D.; Laurent, M.A.; Keller, S.; Chowdhury, S. Dispersion Free 450-V p GaN-Gated CAVETs With Mg-ion Implanted Blocking Layer. *IEEE Electron. Device Lett.* **2017**, *38*, 933–936. [[CrossRef](#)]
16. Ji, D.; Laurent, M.A.; Agarwal, A.; Li, W.; Mandal, S.; Keller, S.; Chowdhury, S. Normally OFF Trench CAVET With Active Mg-Doped GaN as Current Blocking Layer. *IEEE Trans. Electron. Devices* **2017**, *64*, 805–808. [[CrossRef](#)]
17. Ji, D.; Agarwal, A.; Li, W.; Keller, S.; Chowdhury, S. Demonstration of GaN Current Aperture Vertical Electron Transistors With Aperture Region Formed by Ion Implantation. *IEEE Trans. Electron Devices* **2018**, *65*, 483–487. [[CrossRef](#)]
18. Gao, Y.; Ben-Yaacov, I.; Mishra, U.K.; Hu, E.L. Optimization of AlGa_N/GaN current aperture vertical electron transistor (CAVET) fabricated by photoelectrochemical wet etching. *J. Appl. Phys.* **2004**, *96*, 6925–6927. [[CrossRef](#)]
19. Debold, A.; Kotzea, S.; Heuken, M.; Kalisch, H.; Vescan, A. Growth and Characterization of Vertical and Lateral p-n Junctions Formed by Selective-Area p-GaN MOVPE on Patterned Templates. *Phys. Status Solidi* **2018**, *216*, 1800677. [[CrossRef](#)]
20. Sze, S.M.; Ng, K.K. *Physics of Semiconductor Devices*; John Wiley & Sons: Hoboken, NJ, USA, 2006.
21. Witte, W. Building Blocks of Vertical GaN-Based Devices. Ph.D. Thesis, RWTH Aachen University, Aachen, Germany, 2016.
22. Hahn, H.; Lükens, G.; Ketteniss, N.; Kalisch, H.; Vescan, A. Recessed-Gate Enhancement-Mode AlGa_N/GaN Heterostructure Field-Effect Transistors on Si with Record DC Performance. *Appl. Phys. Express* **2011**, *4*, 114102. [[CrossRef](#)]
23. Reuters, B.; Hahn, H.; Behmenburg, H.; Heuken, M.; Kalisch, H.; Vescan, A. Insulating behavior of interfaces in regrown Al_{0.23}Ga_{0.77}N/GaN double heterostructures on Al_{0.07}Ga_{0.93}N back-barrier templates. *Phys. Status Solidi* **2013**, *10*, 799–802. [[CrossRef](#)]
24. Xing, H.; Green, D.S.; Yu, H.; Mates, T.; Kozodoy, P.; Keller, S.; DenBaars, S.P.; Mishra, U.K. Memory Effect and Redistribution of Mg into Sequentially Regrown GaN Layer by Metalorganic Chemical Vapor Deposition. *Jpn. J. Appl. Phys.* **2003**, *42*, 50–53. [[CrossRef](#)]
25. Chowdhury, S.; Swenson, B.L.; Lu, J.; Mishra, U.K. Use of Sub-nanometer Thick AlN to Arrest Diffusion of Ion-Implanted Mg into Regrown AlGa_N/GaN Layers. *Jpn. J. Appl. Phys.* **2011**, *50*, 101002. [[CrossRef](#)]
26. Tomita, K.; Itoh, K.; Ishiguro, O.; Kachi, T.; Sawaki, N. Reduction of Mg segregation in a metalorganic vapor phase epitaxial grown GaN layer by a low-temperature AlN interlayer. *J. Appl. Phys.* **2008**, *104*, 014906. [[CrossRef](#)]
27. Heikman, S.; Keller, S.; Moran, B.; Coffie, R.; DenBaars, S.; Mishra, U. Mass Transport Regrowth of GaN for Ohmic Contacts to AlGa_N/GaN. *Phys. Status Solidi* **2001**, *188*, 355–358. [[CrossRef](#)]
28. Zanato, D.; Gokden, S.; Balkan, N.; Ridley, B.K.; Schaff, W.J. The effect of interface-roughness and dislocation scattering on low temperature mobility of 2D electron gas in GaN/AlGa_N. *Semicond. Sci. Technol.* **2004**, *19*, 427–432. [[CrossRef](#)]
29. Lisesivdin, S.B.; Acar, S.; Kasap, M.; Ozcelik, S.; Gokden, S.; Ozbay, E. Scattering analysis of 2DEG carrier extracted by QMSA in undoped Al_{0.25}Ga_{0.75}N/GaN heterostructures. *Semicond. Sci. Technol.* **2007**, *22*, 543–548. [[CrossRef](#)]

